Hybrid organic–inorganic nanomaterials based on polythiophene dendronized nanoparticles†‡

Rigoberto C. Advincula*

In this work, the synthesis, characterization, and applications of branched oligothiophene dendrons that act as electroactive surfactants for the capping of Au metal nanoparticles and CdSe quantum dots are described. Two distinct methods have been employed for synthesis: a ligand exchange process and a direct-capping synthesis approach. The coverage of the dendrons per nanocrystal, the nature of the surface coordination interactions, and energy transfer interactions were studied in detail using UV-vis absorbance, FT-IR, AFM, TEM, and photoluminescence spectroscopy. The competition/displacement in ligand metathesis is highlighted by the size of the dendron and nature of binding on semiconductor nanocrystals. In the other system using the direct capping method, the size of the Au nanoparticle is mediated by the dimensions of the ligand, *i.e.* alkyl chain spacer and dendron branching or size. These hybrid dendron/nanoparticle complexes are generally very soluble and stable in non-polar solvents. They exhibit energy transfer, surface plasmon resonance effects, and photoinduced charge transfer interactions between the metal/semiconductor and conjugated ligands. Adsorption on mica and graphite surfaces was observed. A one-layer photovoltaic cell was fabricated to demonstrate the potential for device applications.

Introduction

Hybrid organic–inorganic nanomaterials are of high interest because of the possibility of combining the best properties of the two components. They have been the focus of much research for developing new and smart nanocomposite materials. Nanomaterials involving metal nanoparticles display many novel properties, such as high catalytic activity, interesting optical properties, and various physical properties of high interest from a fundamental standpoint.[1] A major advantage is the high surface/volume ratio in nanoparticles. By combining with a polymer matrix or organic component, highly improved mechanical, thermal, and chemical properties are obtained. These interesting properties are often derived from a strategy of maximizing the interface separating the components, determining the percolation threshold of the nanoparticle filler, and optimizing processability of the polymer component. A major objective is to secure a property (or a combination of properties) not available in any of the individual components. Recently, polymer nanocomposites with high electrical and thermal conductivities have also been targeted towards novel electro-optical applications.[2]

Metal-containing organic dendrimers have been extensively investigated because of their potential applications as drug delivery agents, chemical sensors, nanoscale catalysts, and light-harvesting antenna macromolecules.[3] Their design and synthesis is a challenge. These materials can be classified as follows: (1) dendrimers that encapsulate metal ions;[4] (2) dendrimers with metal ions as an integral part of their structure;[5] and (3) dendrimers with peripheral groups that can bind metal ions.[6] Recently, organic chromophores have been attached to the periphery of metal dendrimers to generate novel light-harvesting antenna systems.[7]

Au metal nanoparticles to date have been one of the most well-studied nanoparticle materials not only because of the ease in their synthesis, but because of their surface plasmon properties and amenability to surface functionalization.[8,9] On the other hand, quantum dot semiconductor nanoparticles exhibit interesting quantum size effects and narrow emission bands which are useful to a host of applications; from biomarkers to sensing elements. This includes cadmium chalcogenides, whose electronic transitions can be tuned over the whole visible range, and whose synthesis can be carried out with remarkable size control and very high crystallinity.[10–13]

It has been previously demonstrated that organic dendron ligands can act as very good stabilizers for metal and semiconductor nanoparticles.[14] It was supposed that the steric crowding of the dendron provides a closely packed but thin ligand shell in contrast to a shell formed by ligands with long and flexible alkyl chains. This steric crowding is deemed to be ideal for filling the spherical ligand layer because the dendron ligands can naturally pack in a cone shape on the surface of the nanoparticle. Inter- and intramolecular entanglement of the dendrons with relatively flexible branches may further slow the diffusion of small molecules or ions from the bulk solution to the interface between a nanocrystal and its ligands. In the past, our group has reported the synthesis and characterization of conjugated polythiophene dendrons and dendrimers which exhibited broad absorbance and band gap tunability by varying the generation and connectivity

Department of Chemistry and Department of Chemical Engineering, University of Houston, Houston, TX, 77204, USA. E-mail: radvincula@uh.edu; Fax: +1 713-743-1755; Tel: +1 713-743-1760

of the macromolecule.[15] These materials exhibited interesting nanostructures on mica and graphite surfaces due to π–π and van der Waals interactions. This included 2-D crystallization and nanowire formation.

In this article, we describe and review strategies and results for combining metal/semiconductor nanoparticles with attached dendronized polythiophene ligands that exhibit energy transfer characteristics.[16] Using primarily "grafting onto" methods, these dendronized ligands were separately synthesized and attached through ligand exchange or directly used as stabilizing surfactants during the reduction stage to form hybrid organic–inorganic nano-materials. Our interest mainly lies in understanding energy transfer and electron transport properties in order to harness their utility in future sensor and device applications. We will describe the size and distance dependent properties of these thiophene dendrons on metal/semiconductor nanoparticles with applications towards photovoltaics for example. There is a need to rationally develop design and synthesis protocols in order to explore the advantages of these hybrid materials. In addition, the electroactive dendrons should provide the nanoparticles with better miscibility in a conjugated polymer matrix for the preparation of electro-optically active nanocomposites. Other groups have reported a "grafting from" approach to these materials based on direct growth of the linear conjugated oligomers or polymers from the surface of the nanoparticles.[17]

Experimental

Materials

Thiophene dendrons (Fig. 1 and 2) were synthesized using a convergent synthesis approach based on an AB₂ type monomer: 2,3-dibromothiophene as reported earlier.[15] A number of metal mediated-cross coupling reactions based on Kumada and Stille coupling as well as lithiation reactions were utilized in a rational route towards generational growth in these dendrons. The terminal end-groups were functionalized to contain phosphonic acid and thiol for binding to the surface of the nanoparticles. 11-Mercaptoundecylamine was synthesized as reported in the literature (Fig. 2).[18] THF and toluene were freshly distilled from sodium benzophenone. Spectroscopic-grade solvents from Aldrich were used for spectral measurements. All other commercially available reagents were purchased from Aldrich and used as received. Silica gel (60 Å, 32–63 μm, Standard Grade) was purchased from Sorbent Technologies, Inc. (Atlanta, GA). More details are given in the ESI.‡

CdSe nanoparticle synthesis

The CdSe nanoparticles were synthesized and purified using a modification of a previously described approach.[13,14,29] In this procedure, trioctylphosphine oxide (TOPO) (3.0 mmol), octade-cylamine (11.8 mmol), hexylphosphonic acid (0.8 mmol) and CdO (0.4 mmol) were added to a Schlenk flask and heated under vacuum at 80 °C. The flask was backfilled with N₂ and heated to ~320 °C until a colorless solution was obtained. The temperature was lowered to 270 °C and 2.5 mL of Se (in 0.2 M in trioctylphosphine (TOP)) was added. The reaction (heating) was stopped when the desired size of nanoparticles was obtained. After
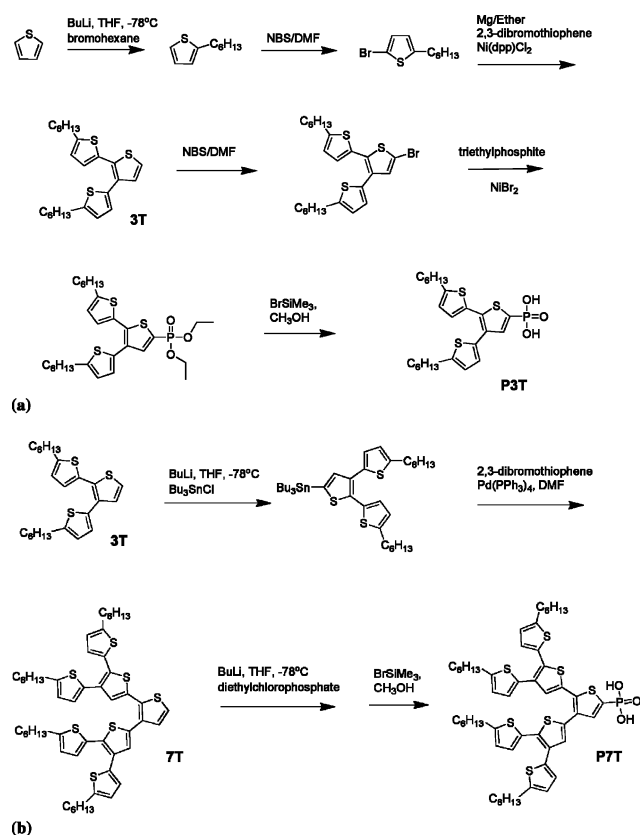
Fig. 1 (a) P3T and (b) P7T. Synthesis routes for phosphonic acid terminated thiophene dendron ligands. Reference 16.

the solution cooled to about 60 °C, ~20 mL of degassed CHCl₃ was added to the flask and the solution was centrifuged to remove unreacted precursors. The nanoparticles were then precipitated with degassed methanol where centrifugation and decantation were performed to remove any unbound organic material. The process of redispersal and precipitation was repeated several times to ensure removal of excess ligands. The nanoparticles were then used immediately.

Ligand exchange with the dendron surfactant

For ligand exchange (Fig. 3), the TOPO capped nanoparticles and an excess of the polythiophene dendron surfactants were co-dissolved in choloroform and allowed to stir for at least 24 hours under an inert atmosphere.[16] The product was then precipitated in methanol to remove the displaced TOPO and any excess surfactant. Redispersion, excess surfactant, and precipitation was repeatedly done in choloroform and methanol until no excess ligand was detected by UV-vis absorption of the wash solution. After final washing, the nanoparticles were dispersed in choloroform and stirred for at least 24 hours under an inert atmosphere prior to usea. The work-up procedure was the same for P3T or P7T as described above. An alternative procedure involved the use of an intermediate pyridine displacement step of the TOPO.

Direct synthesis of dendronized Au nanoparticles

For the direct synthesis of dendronized Au nanoparticles, firstly, a stock solution of 100 mM didodecyldimethyl ammonium bromide
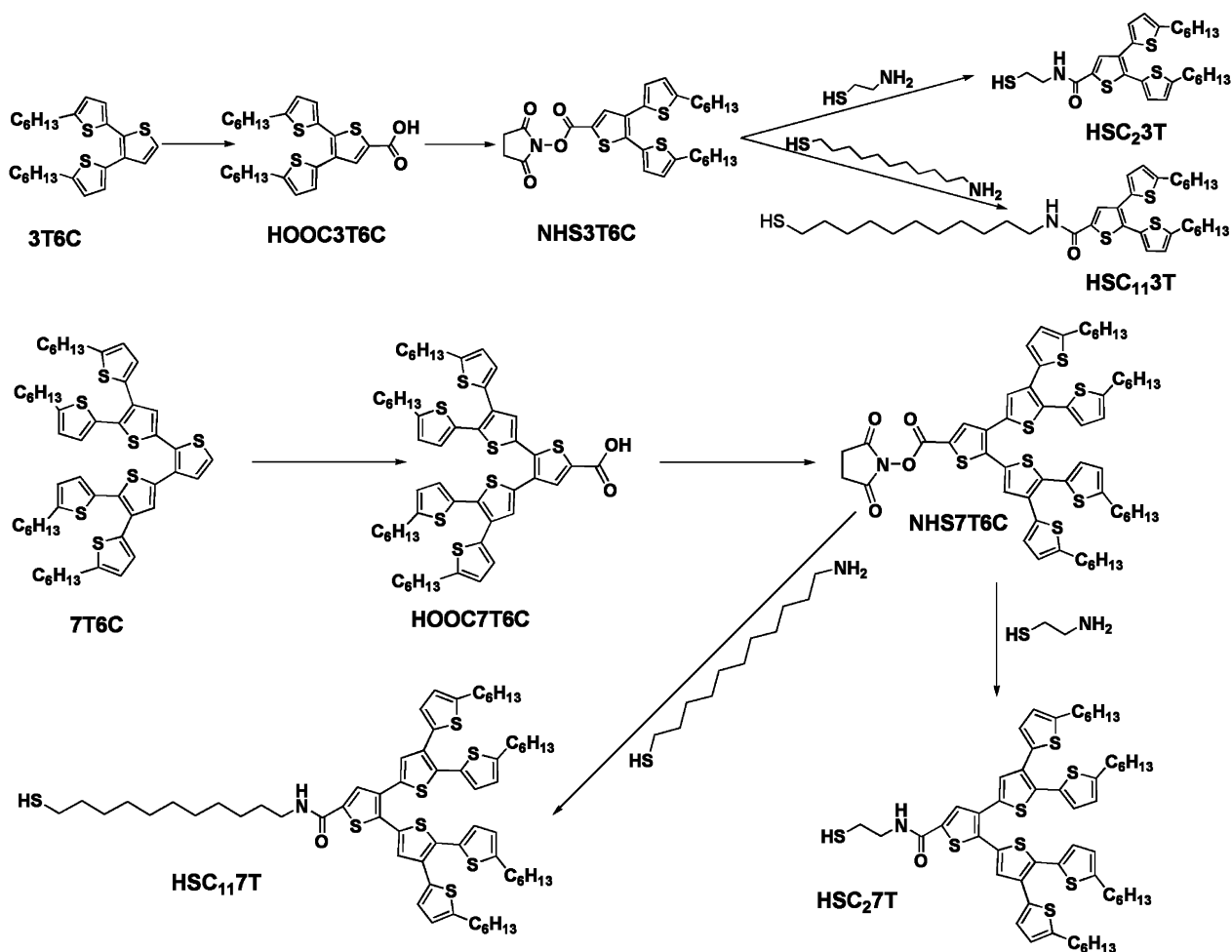
Fig. 2 Synthesis routes for thiol terminated thiophene dendron ligands showing alkyl spacer variants.
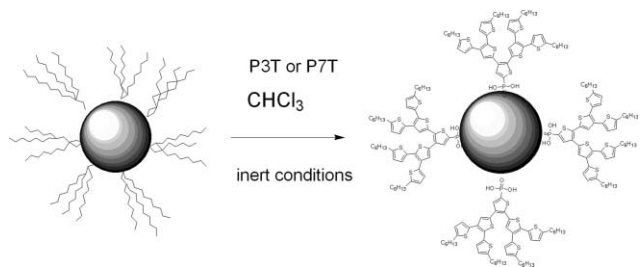
Fig. 3 Diagram showing the ligand exchange process for replacing TOPO with the polythiophene dendrons functionalized with phosphonic acid.

(DDAB) was prepared. Then 15.0 mg AuCl₃ was dissolved in 5.0 mL of DDAB solution by sonication leading to an orange-red color. To this solution was added a solution of one equivalent of the dendritic thiol in toluene (2.0 mL). After 15 min of stirring, 50 mg of tetrabutylammonium borohydride (TBAB) reducing agent in 2.0 mL DDAB solution was injected and the mixture was stirred overnight. The toluene was removed in a rotary evaporator at 50 °C and the excess dendritic thiol in the residue was removed by repeated dissolution and precipitation. The same procedure was used for the HSC-2-3T, HSC-2-7T, HSC-11-3T and HSC-11-7T dendronized thiol ligands. More details about the thiol ligand syntheses are given in the ESI.‡

Instrumentation

Nuclear magnetic resonance (NMR) spectra were recorded on a General Electric QE-300 spectrometer operating at 300 MHz for ¹H and 75 MHz for ¹³C nuclei. UV-vis spectra were recorded on an Agilent 8453 UV-visible Spectrometer and photoluminescence (PL) spectra on a PerkinElmer LS 45 Luminescence Spectrometer. FT-IR spectra were obtained using a FTS 7000 Spectrometer Digilab (Varian), Randolph, MA equipped with a liquid N₂-cooled MCT detector. KBr pellets were prepared by first mixing the sample solutions with KBr, removing solvents under vacuum and then pressing the KBr using a 10-ton hydraulic press. Atomic force microscopy (AFM) imaging was performed in air with a PicoSPM II, PicoPlus, Molecular Imaging (Agilent) in the non-contact Magnetic AC mode (MAC Mode). Type II MAC-levers with a spring constant of 2.8 nN M⁻¹ and resonance frequency of 75 kHz with about 10 nm tip radius were used for all scans. Samples were prepared by dropcasting about 2 mg L⁻¹ solutions in toluene onto a freshly cleaved HOPG or mica substrate spinning at about 1000 rpm. Spin rate and concentration were optimized for the different solutions in order to get the best AFM images. All solutions were passed through two 0.2 μM hydrophobic fluoropore (PTFE) filters (Millex, Millipore) as they were cast. The surface was washed with deionized water, methanol, and then dried under

a stream of N₂. Transmission electron microscopy (TEM) was performed on a JEOL 2000 FX microscope operating at 200 kV. Samples for TEM were prepared by drop-casting one drop of a ~0.1 mg mL^{-1} nanoparticle solution in CHCl$_3$ onto standard carbon-coated Formvar films on copper grids (300 mesh) and drying in air for 30 min. The average cluster diameters were obtained using the ImageJ software.

Device fabrication

A solution of the hybrid nanomaterial were spin cast onto indium tin oxide (ITO)-coated glass substrates (cleaned by the RCA method)[19] at 1200 rpm for 60 seconds and the thickness obtained by profilometry. Al (100 nm) was evaporated on the active layer at a rate of 0.5–1.0 nm s^{-1}. The active area of the device was 0.23 cm^2. Current–voltage characteristics were measured using a Keithley 236 Source Measure Unit with a Oriel Hg–Xe Lamp hooked up to a monochrometer. The incident power (P_{in}) was 0.14 mW cm^{-2}. Power conversion efficiency (η_e) was calculated according to the following equation:

$$\eta_e = I_{sc} \times V_{oc} \times FF/I_{in}$$

where I_{sc} is the short-circuit current density in mA cm^{-2}, V_{oc} is the open-circuit voltage and I_{in} is the intensity of irradiating light in mW cm^{-2}, and FF (fill factor) is defined as follows:

$$FF = \max\{I \times V\}/I_{sc} \times V_{oc}$$

Results and discussion

Synthesis and characterization of dendronized CdSe nanoparticles

Several methods were utilized to characterize the formation of the hybrid nanoparticles: FT-IR was primarily use to identify ligand exchange.[16] On the other hand the energy transfer properties were probed by absorbance and PL measurements. The dimensions of the nanoparticle were probed by AFM.

Synthesis of the dendrons. The full procedure for the synthesis of the dendrons and their characterization have been previously reported.[16] This involved a generational dendron growth employing Stille and Kumada coupling reactions, the last step being phosphonic acid group termination. Reactions involving the convergent approach to dendrons are facile and easily characterized by NMR and MALDTI-TOF MS. The full procedure for the thiol terminated dendron will be reported in another publication.[28] Some details can be obtained from the accompanying ESI.‡

FTIR spectroscopic analysis. Analysis of the FTIR absorbance spectra was utilized to monitor the ligand exchange process by monitoring specific frequencies associated with TOPO, P3T, P7T, and the CdSe nanoparticle complex at specific stages of the exchange process (Fig. 4). On the "as synthesized" nanoparticle, the P=O stretch of the TOPO ligand at 1149 cm^{-1} is broadened into three frequencies: 1166, 1095, and 929 cm^{-1} indicative of multidentate coordination through occupation of bridging positions over the Cd sites.[20,21] The rest of the peaks in the spectrum of TOPO capped nanocrystals do not change with respect to position, shape, or intensity compared to TOPO ligand. This implied that the other groups were not in contact with the surface of the nanocrystal. On the other hand, the spectrum of P3T showed
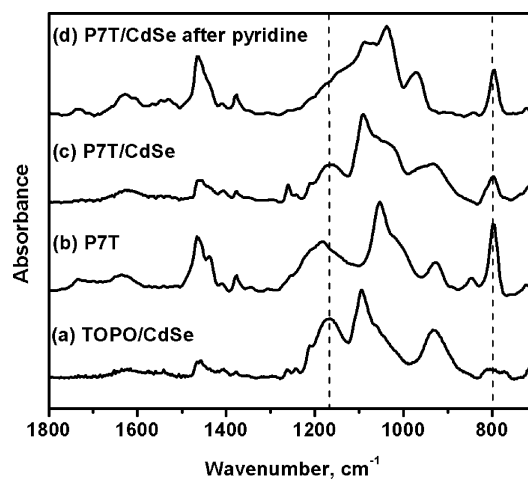
Fig. 4 FT-IR spectra in the P=O stretching region of (a) TOPO capped CdSe, (b) P7T ligand, (c) P7T/CdSe, (d) P7T/CdSe after pyridine exchange. Reference 16.

peaks at the P=O (1180 cm^{-1}), Ar–P–O (1065 cm^{-1}), P–O–H$_{(as, s)}$ (1016, 997 cm^{-1}), and Ar–P–O (922 cm^{-1}) frequencies (see ESI Fig. 1‡).[22–24] The C–H out of plane vibration of the substituted thiophene ring is assigned to 804 cm^{-1}. For the P3T/CdSe complex after exchange with the TOPO capped nanoparticles, the peaks are broadened significantly and resemble a combination of P3T and TOPO indicating an inefficient exchange. The spectrum of P7T gave P=O (1183 cm^{-1}), Ar–P–O (1053 cm^{-1}), P–O–H (1011 cm^{-1}), and the Ar–P–O (929 cm^{-1}) (Fig. 4). The peaks are again broadened significantly probably due to intermolecular hydrogen bonding between molecules. The C–H out of plane vibration of the substituted thiophene ring is assigned at 796 cm^{-1}.[25,26]

For the P7T/CdSe complex after exchanging directly from TOPO/CdSe and the pyridine capped nanocrystals, a change in intensities of the P=O was observed. The peak at 796 cm^{-1} is evident of the binding of P7T to the nanocrystal surface. The intensity of the P=O stretching vibration at 1183 cm^{-1} decreased due to Lewis acid coordination to Cd atoms. The P–OH band remained, indicating the absence of condensation, and is shifted slightly to higher wavenumbers. Both exchange processes (for P3T and P7T) were also verified by NMR primarily by dissolving first the nanoparticle core and isolating the ligand.

AFM imaging. From the AFM imaging of single P7T/CdSe nanocrystals dropcast on mica, the particles were found to be nearly monodispersed, with an average height of 3.84 nm (Fig. 5). This value is based on the height profile of 35 sampled particles. This dimension is consistent with the structure of the dendrons and the average size of the nanoparticle based on the absorption measurements. Previous investigations of the polythiophene dendrimers alone revealed similar dispersion properties and aggregation behavior on mica surfaces.[15]

Absorption and photoluminescence behavior.

P3T derivative. Absorption properties showed that P3T has an absorption maximum at 249 nm with two shoulders at 270 and 330 nm (Fig. 6). The specific absorption coefficient was determined to be $\varepsilon = 11\,400$ L mol^{-1} cm^{-1} at 330 nm using the Beer–Lambert law. A significant Stokes shift on the PL was observed with the emission centered at 452 nm with a quantum yield of ~6% in
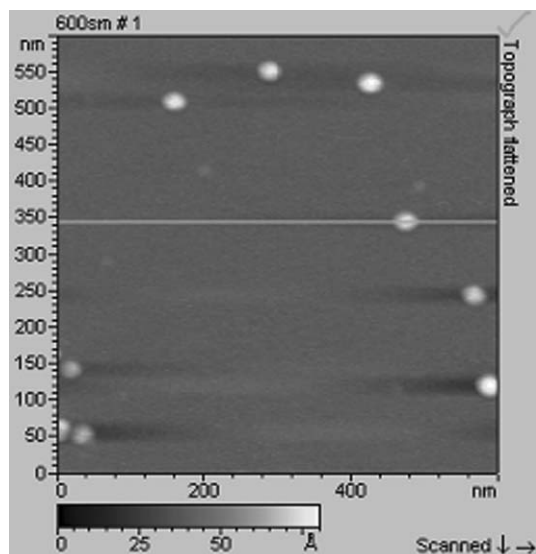
Fig. 5 AFM image of drop-cast nanoparticles on mica surface. Reference 16.
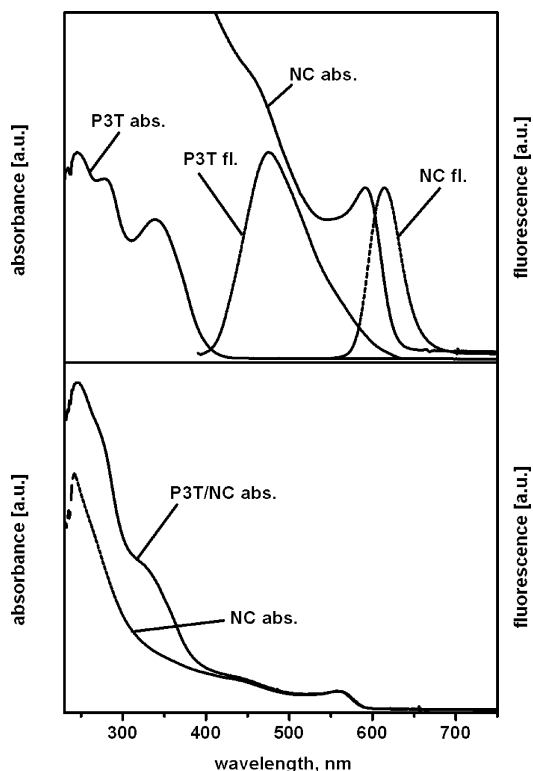
Fig. 6 Absorption and PL spectra of P3T and NC (top) in CHCl$_3$. The bottom graph is of the P3T/NC complex. The fluorescence (fl.) for both P3T and NC is completely quenched in the complex. Deconvolution yields about 53 P3T molecules per NC (reference 16).

CHCl$_3$ with respect to diphenylanthracene in cyclohexane. For the CdSe nanocrystals, the absorbance maximum at the first excitonic peak was 556 nm with the PL maximum at 576 nm. The quantum yield of the TOPO-capped CdSe nanocrystals was ~5%. Size and extinction coefficients at the first excitonic absorption peak for the nanocrystals were calculated using empirical fitting functions based on the literature.[27] From this, a diameter of 3.17 nm and $\varepsilon =$

124 320 L mol^{-1} cm^{-1} at 556 nm can be assigned. After exchange, the absorbance resembles a superposition of the two species with no other apparent peaks or features present (Fig. 6). No change in the first excitonic absorption was observed. The spectrum can be deconvoluted using the molar absorption coefficients of the two species and subtracting out the nanoparticle absorbance revealing an average of 53 P3T molecules per nanocrystal (NC) (for 3.17 nm diameter). For the PL behavior of the CdSe/P3T, the fluorescence of the two species is completely quenched (not shown).

P7T derivative. The absorbance and emission spectra of P7T likewise are consistent with P3T (see ESI‡). The absorbance is broader with a maximum at 255 nm and several peaks at 280, 309, 368 and a tail ending around 470 nm is observed. The broadening is due to the different conjugation pathways between the thiophene rings.[15] The emission spectrum has a maximum at 521 nm and the quantum yield is 25%. The specific absorption coefficient was 23 300 L mol^{-1} cm^{-1} at 280 nm. The absorbance and PL of the P7T/nanocrystal complex showed similar behavior as with the P3T exchange. The absorbance of the nanocrystals before and after exchange was found to be $\lambda_{max} = 536$ nm, diameter = 2.79 nm. After deconvolution, it was determined that an average of 30 P7T dendrons coated each nanocrystal. As with the P3T, the PL of both the nanocrystals and the P7T is completely quenched. To ensure that the phosphonic acid binding moiety was completely passivating the surface and not just inducing surface defects that could quench fluorescence, the exchange of a phenyl phosphonic acid derivative was carried out under the same protocol. We observed the enhancement of the fluorescence of the nanocrystals after the TOPO exchange. Thus the quenching could be the result of electron transfer between the ligand and the nanocrystals.

Photovoltaic device. We investigated possible device applications by studying the effect of non-radiative energy transfer, *i.e.* direct photocurrent conversion, by constructing a simple photovoltaic device. Based on the PL behavior, the dendron/nanocrystal complexes should undergo photoexcited charge transfer between the two species. The dendrimer itself exhibits photocurrent behavior with a Shottky conduction type of behavior based on our previous studies.[15c] In this case, current–voltage curves were measured for a one-layer device prepared by spin-coating P7T/CdSe nanocrystals on ITO. The results showed the following characteristics for the device: open circuit voltage, $V_{oc} = 0.6$ V, short-cricuit current density, $I_{sc} = 1.56 \times 10^{-6}$ A cm^{-2}, fill factor, FF $= 0.3$, incident power, $P_{in} = 0.1$ mW cm^{-2}, and power conversion efficiency, $\eta_e = 0.29\%$. Based on these results, it can be expected that electron transport in this device will be limited by the small size of the nanocrystals. It is possible that the efficiency can be further optimized by increasing the size and changing the shape of the nanocrystals.

Synthesis and charaterization of dendronized Au nanoparticles

We have previously demonstrated that thiophene dendrons are excellent light-harvesting antenna macromolecules and have unique self-assembly properties.[15] In order to investigate systematically the effect of alkyl chain length and thiophene dendron size on the Au nanoparticle size and energy transfer efficiency, four dendritic thiol ligands were synthesized. The full synthesis protocol and characterization will be reported elsewhere.[28] Preliminary data is given in the ESI.‡ The hybrid nanoparticles were directly

synthesized and purified using a single-phase approach.[29] In this case, the thiol functionalized dendrons were directly utilized as ligands. AuCl$_3$ dissolved in toluene with DDAB was reduced by TBAB in the presence of dendritic thiol ligands, which is equivalent to the last step in a conventional convergent dendrimer synthesis. The nanoparticles are freely soluble in CHCl$_3$, toluene, diethyl ether and hexane, but insoluble in methanol and ethanol. Similar to the nanoparticles coated with alkanethiolate ligands, these nanoparticles are very stable in solution or as solvent-free powders. No decomposition or precipitation from their solutions in toluene was observed over six months.

TEM analysis and AFM imaging. TEM imaging showed that these nanoparticles are relatively small and have a quite uniform core size (Fig. 7). Core sizes for Au–SC-2-3T, Au–SC-11-3T, Au–SC-2-7T and Au–SC-11-7T are 2.88 ± 0.69, 4.09 ± 1.03, 3.84 ± 0.97 and 4.68 ± 1.22 nm, respectively. The average core size of the hybrid nanoparticles increases while the size distribution becomes broader as the size of thiophene dendron increases. Moreover, core sizes and size distribution depended on the dendron size more sensitively for short alkyl chain ligands (HSC-2-3T and HSC-2-7T) than long alkyl chain ligands (HSC-11-3T and HSC-11-7T). This trend is expected because the steric congestion caused
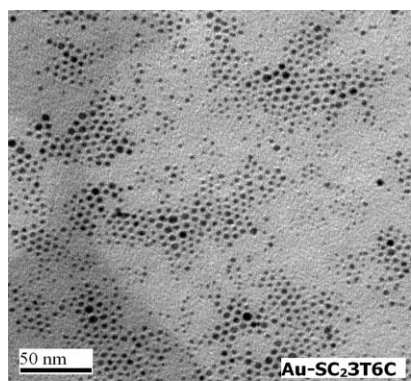
(a)
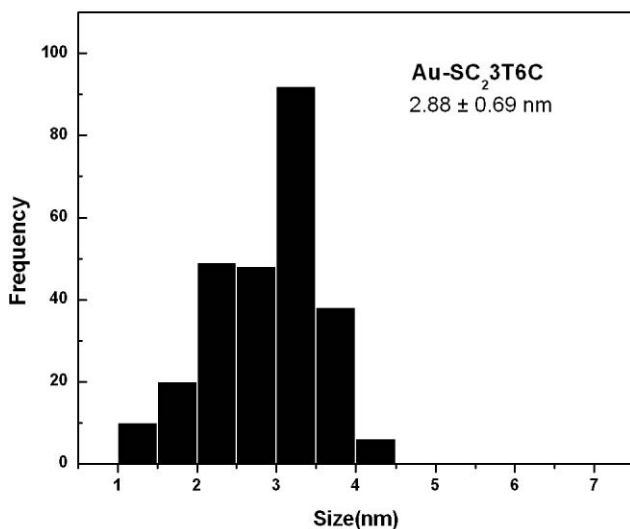
(b)

Fig. 7 TEM Image of Au–SC-2-3T and histogram distribution.

by bigger dendrons becomes more prominent for short alkyl chain ligands. The increased steric congestion in fact leads to slower reaction with the growing Au nanoparticles, resulting in the formation of larger gold clusters and broader size distribution. In contrast, smaller core size and more narrow size distribution of the alkanethiolate functionalized nanoparticles are expected when sterically bulkier ligands are used.[30] The dependence of core sizes and size distribution on alkyl chain length is similar to that observed with other ligand capped nanoparticles.[31] The alkyl chain length has more effect on core sizes and size distribution for smaller dendron ligands (HSC-2-3T and HSC-11-3T). Although only one set of reaction conditions was used in this study, it is expected that entirely different size distribution patterns would result under other reaction conditions. These nanopartilces can form aggregates of very uniform size both on HOPG and mica as observed by AFM (see ESI, Fig. 9‡).

UV-vis absorbance measurements. UV-vis was used to monitor the synthesis and purification of the hybrid nanoparticles. The surface plasmon bands at ~530 nm clearly indicated the formation of Au nanoparticles (Fig. 8). Moreover, Au–SC-2-3T and Au–SC-11-3T showed characteristic absorption bands of their ligands at ~349 nm. However, it is not obvious for Au–SC-2-7T and Au–SC-11-7T because their ligands have almost featureless absorption (see ESI,‡ Fig. 5). Care was taken to make sure that no free ligands remained in the nanoparicles. For all the hybrid nanoparticles, the relative intensities of the plasmon band to ligand absorption band increased compared to those of the reaction mixtures due to the removal of free ligands. Seemingly, the plasmon band maxima are not very consistent with TEM measurements in terms of size correlation. A slight agglomeration may have occurred during purification as indicated by the red-shift of plasmon band maxima. This phenomenon is probably related to differences in interdigitation[32] of hexyl chain domains for different ligands.

IR and NMR spectral analysis. IR spectra of nanoparicles provided very useful information about the conformation and ordering of the alkyl chain on the metal surface (see ESI,‡ Fig. 6). First of all, a significant decrease in the SH stretching region,
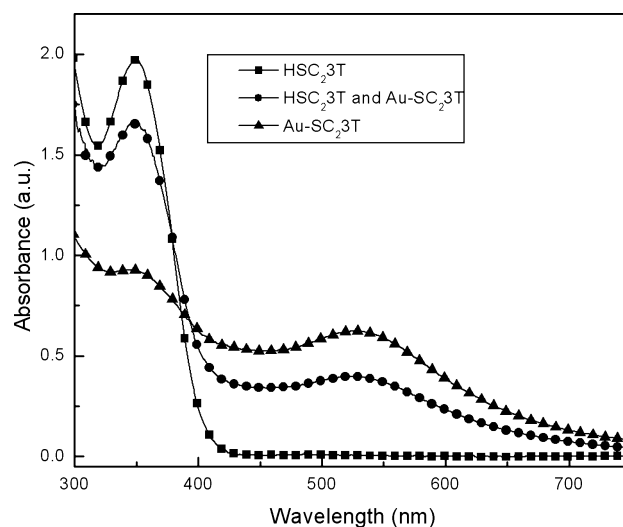
Fig. 8 Absorbance spectra of Au nanoparticle, SC-2-3T, Au–SC-2-3T solutions.

3200–3600 cm^{-1} was observed for all dendron derivatives when bound on the Au nanoparticles. Except for relatively less intense amide I band at about 1650 cm^{-1}, the IR spectra of all the hybrid nanoparticles and dendritic ligands were almost identical. This indicates that the "alkyl spacers" are relatively disordered for all the nanoarticles. ^{1}H NMR spectra of the nanoparticles are broadened significantly relative to those of their corresponding free ligands, which is indicative of signficant crowding and trapping of different dendron conformers. However, the integrations for the proton signals of Au–SC-11-3T and Au–SC-11-7T were found to remain accurate.

PL spectra of the hybrid nanoparticles. The emission spectra of the hybrid nanoparticles retained the same shape and peak positions as those of their ligands, but the intensities of the emission were significantly quenched (Fig. 9 and ESI, Fig. 8‡). To separate the effect of decreased absorption by the attached dendritic ligands in competition with the Au core, we prepared mixtures of dendritic ligands and 6 nm Au nanoparticles capped with decanoic acid, which are optically matched to the nanoparticle solutions. The emission intensities decreased by 90, 70, 85 and 67% for Au–SC-2-3T, Au–SC-11-3T, Au–SC-2-7T and Au–SC-11-7T, respectively. In this case, the energy transfer efficiency decreases as the chain length and dendron size increase. The distance-dependent quenching is similar to that observed in other chromophore-functionalized Au nanoparticles.[33] As suggested by Kamat et al.,[34] densely packed chromophores result in a dramatic suppression in the quenching. Therefore, a more dense packing of bigger dendrons on Au nanoparticle surfaces could be used to explain the dependence of energy transfer efficiency on the dendron size. Because of this moderate quenching, these hybrid nanoparticles have some advantages over most chromophore-functionalized Au nanoparticles for applications in optoelectronic devices and photonic materials.
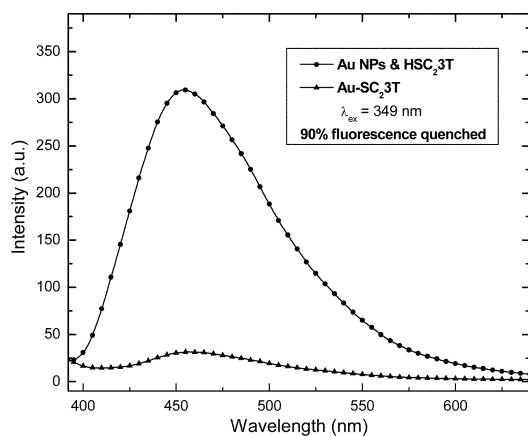
Fig. 9 PL spectra of Au–SC-2-3T showing the high degree of quenching.

Conclusions

In summary, we have successfully demonstrated the synthesis and characterization of nanoparticle-cored thiophene dendrons with metal and semiconductor nanoparticles. We also systematically studied the effect of alkyl chain length and dendron size on nanoparticles size and energy transfer efficiency. These nanomaterials, possessing quantum dot or metal nanoparticles at the core and thiophene dendrons radially attached to the core, were analyzed by TEM, UV, IR and ^{1}H NMR. The quantum dot nanoparticles were predictable in size and emission. Au nanoparticles are small and quite uniform in size based on the plasmon band and by TEM measurements. Nanoparticle size, size distribution and energy transfer efficiency (quenching) depended sensitively on both alkyl chain length and dendron size. Based on the observed properties, these hybrid nanoparticles should have potential applications in light-harvesting systems, optoelectronic devices as well as in catalysis

References

1 W. Haperin, *Rev. Mod. Phys.*, 1986, **58**, 533.
2 V. Colvin, M. Schiamp and P. Alivisatos, *Nature*, 1994, 370.
3 G. Newkome, C. Moorefield and F. Vögtle, *Dendrimers and Dendrons*, Wiley-VCH, Weinheim, Germany, 2001.
4 L. Zhou, D. Russel, M. Zhao and R. Crooks, *Macromolecules*, 2001, **34**, 3567.
5 K. Gopidas, J. Whitesell and M. Fox, *J. Am. Chem. Soc.*, 2003, **125**, 6491.
6 L. Balogh and D. Tomalia, *J. Am. Chem. Soc.*, 1998, **120**, 7355.
7 X. Zhou, D. Tyson and F. Castellano, *Angew. Chem., Int. Ed.*, 2000, **39**, 4301.
8 M. Daniel and D. Astruc, *Chem. Rev.*, 2004, **104**, 293.
9 C. Burda, X. Chen, R. Narayanan and M. A. El-Sayed, *Chem. Rev.*, 2005, **105**, 1025.
10 Z. Peng and X. Peng, *J. Am. Chem. Soc.*, 2001, **123**, 183.
11 X. Peng, *Chem.–Eur. J.*, 2002, **8**, 334.
12 C. Murray, D. Norris and M. Bawendi, *J. Am. Chem. Soc.*, 1993, **115**, 8706.
13 X. Peng, J. Wickham and P. Alivisatos, *J. Am. Chem. Soc.*, 1998, **120**, 5343.
14 W. Guo, J. Li, Y. Wang and X. Peng, *J. Am. Chem. Soc.*, 2003, **125**, 3901.
15 (*a*) C. Xia, X. Fan, J. Locklin and R. Advincula, *Org. Lett.*, 2002, **4**, 2067; (*b*) C. Xia, X. Fan, J. Locklin, R. Advincula, A. Gies and W. Nonidez, *J. Am. Chem. Soc.*, 2004, **126**, 8735; (*c*) K. Shinbo, Y. Ikeda, C. Xia, K. Kato, F. Kaneko and R. Advincula, *Curr. Appl. Phys.*, 2005, **5**, 314.
16 J. Locklin, D. Patton, S. Deng, A. Baba, M. Millan and R. Advincula, *Chem. Mater.*, 2004, **16**, 587.
17 H. Skaff, K. Sill and T. Emrick, *J. Am. Chem. Soc.*, 2004, **126**, 11322.
18 J. Tien, A. Terfort and G. Whitesides, *Langmuir*, 1997, **13**, 5349.
19 W. Kern, *Semicond. Int.*, 1984, **94**.
20 J. Katari, V. Colvin and P. Alivisatos, *J. Phys. Chem.*, 1994, **98**, 4109.
21 M. Eilon, T. Mokari and U. Banin, *J. Phys. Chem. B*, 2001, **105**, 12726.
22 D. Corbridge, Phosphorus Compounds, in *Topics in Phosphorous Chemistry*, Wiley & Sons, New York, 1969, vol. 6.
23 R. Artzi, S. Daube, H. Cohen and R. Naaman, *Langmuir*, 2003, **19**, 7392.
24 J. Chalmers and P. Griffiths, *Handbook of Vibrational Spectroscopy*, Wiley, Chichester, 2002.
25 S. Hotta, S. Rughooputh, A. Heeger and F. Wudl, *Macromolecules*, 1987, **20**, 212.
26 G. Socrates, *Infrared Characteristic Group Frequencies*, Wiley, Chichester, 1980.
27 W. Yu, L. Qu, W. Guo and X. Peng, *Chem. Mater.*, 2003, **15**, 2854.
28 S. Deng and R. Advincula, to be submitted.
29 N. Jana and X. Peng, *J. Am. Chem. Soc.*, 2003, **125**, 14280.
30 T. Yonezawa, K. Yasui and N. Kimizuka, *Langmuir*, 2001, **17**, 271.
31 J. Martin, J. Wilcoxon, J. Odinek and P. Provencio, *J. Phys. Chem. B*, 2000, **104**, 9475.
32 A. Badia, L. Cuccia, L. Demers, F. Morin and R. Lennox, *J. Am. Chem. Soc.*, 1997, **119**, 2682.
33 A. Aguila and R. Murray, *Langmuir*, 2000, **16**, 5949.
34 P. Kamat, S. Barazzouk and S. Hotchandani, *Angew. Chem., Int. Ed.*, 2002, **41**, 2764.